Spectral analysis of wave propagation through rows of scatterers via random sampling and a coherent potential approximation.

L. G. Bennetts* & M. A. Peter[†‡]

* School of Mathematical Sciences, University of Adelaide, Adelaide 5005, Australia

† Institute of Mathematics, University of Augsburg, 86135 Augsburg, Germany

‡ Augsburg Centre for Innovative Technologies, 86135 Augsburg, Germany

May 8, 2013

Abstract

A method is proposed to determine the modal spectra of waves supported by arrays, which are composed of multiple rows of scatterers randomly disordered around an underlying periodic configuration. The method is applied to the canonical problem of arrays of identical small acoustically-soft circular cylinders, and disorder in the location of the rows. Two different approaches are adopted to calculate the modes: (i) forming an ensemble average of the modes from individual realisations (loosely: extract information, then average); and (ii) extracting the modes from the ensemble average wave field (loosely: average, then extract information). Differences in the attenuation rates predicted by the two approaches, which cannot be attributed to numerical errors, are found for problems involving multiple wave directions and large disorder. A form of the coherent potential approximation (CPA) is also devised. Comparisons of the CPA to the results given by random sampling show that it gives high accuracy.

1 Introduction

The investigation reported herein is concerned with multiple scattering of linear time-harmonic waves in two-dimensions. In this context, randomly disordered multiple-row arrays have been used to model photonic devices, e.g. McPhedran et al. [5], and water-wave propagation through fields of floating bodies, e.g. Peter & Meylan [6]. Each row in the array contains an infinite number of scatterers and satisfies a periodicity condition, i.e. a constant spacing of the scatterers. (The rows are referred to as diffraction gratings in some applications.) Wave interactions between the rows are confined to a finite set of propagating waves by enforcing a consistent periodicity of the rows in the array. The number of wave directions is determined by the incident wave field and the periodicity of the rows. Wave propagation through the arrays can therefore be calculated at a relatively low cost, whilst allowing for some directional evolution of the wave with distance into the array.

For the water-wave application, in particular, the quantity of interest is the expected rate of exponential wave attenuation, which is induced by the disorder. McPhedran et al. and Peter &

Meylan, e.g., identified a solitary attenuation rate for each problem from the ensemble average of the transmitted energy, i.e. the sum over all transmitted wave directions, with respect to the disorder. This is, however, an oversimplification for problems in which more than one wave direction exists. An incident wave will excite a number of modes in the array, equal to the number of wave directions between rows. Each mode attenuates at a different rate, and also has an associated energy flux.

The modal spectrum is studied here for the canonical problem of an array composed of identical small acoustically-soft circular cylinders, and disorder in the location of the rows around an underlying periodic structure. The modes are sought using two approaches. The first approach is referred to as a localisation approach, in reference to the explanation of the phenomenon given by Berry & Klein [2]. It is closely related to the approaches adopted in McPhedran et al. and Peter & Meylan. In the localisation approach the properties of the modes are calculated as the ensemble averages of properties displayed in individual realisations. The second approach is to extract average properties from the ensemble average wave field, and is based on effective media theory. Numerical algorithms are developed to implement the two approaches, in which the ensembles are approximated via random sampling. Results obtained using the algorithms indicate that the two approaches predict almost identical attenuation rates in most cases, but that they diverge from one another for large disorder when multiple wave directions exist. The inability of the localisation approach to produce a reliable approximation of the energy fluxes of the modes is also identified. As part of the analysis of the results, the relative performance of the numerical algorithm for each approach is discussed.

A form of the coherent potential approximation (CPA) is also derived for the multiple-row problem. The CPA predicts the modes of the disordered array from an individual cell in the array, which, for the problem under consideration, contains a single row and the surrounding free space. Use of the CPA is motivated by the work of Maurel et al. [4], who showed that it is accurate for small perturbations of a one-dimensional periodic array. The CPA derived here differs from and/or extends that of Maurel et al. in two ways. Firstly, it is applied to problems involving multiple wave directions. Secondly, it is applied without any assumption on the magnitude of the disorder, which necessitates the use of a minimisation routine in the solution method. Numerical results are used to validate the CPA via comparisons to the effective media random sampling approach.

2   Multiple-row problem

Wave propagation is considered in an infinite two-dimensional domain, which is defined by the Cartesian coordinates (x, y). An infinite array of scatterers, arranged into rows, occupies the domain. Without loss of generality, the rows are aligned to be parallel to the x-axis. The domain is otherwise occupied by free space. Under the usual assumptions of linear motions, of a prescribed angular frequency ω, the velocity field may be obtained as the real part of the (spatial) gradient of the scalar field $\phi(x, y)\mathrm{e}^{-\mathrm{i}\omega t}$. The complex function ϕ is a velocity potential and is the principal unknown of the problem. At all points in the domain not occupied by scatterers, the velocity potential satisfies Helmholtz equation

$$\nabla^2 \phi + k^2 \phi = 0,$$

where $\nabla^2 \equiv \partial_x^2 + \partial_y^2$ is the Laplacian operator, and k is the wave number of free space.

2.1 Scattering by a row of small sound-soft cylinders

Each row in the array consists of an infinite number of identical and evenly spaced scatterers. The focus of the present investigation is on how interactions between rows affect wave propagation characteristics. Simple isotropic point scatterers are therefore chosen — specifically, small acoustically-soft circular cylinders. The description 'small' is relative to the wavelength, i.e. $ka \ll 1$, where a is the radius of the cylinders. For the numerical results presented in this investigation $ka = 10^{-2}$. It will be shown in § 3.2 that rows of isotropic point scatterers exhibit an interesting property with respect to wave attenuation.

An analytic solution for wave scattering by a single row of acoustically-soft cylinders is given by Linton & Martin [3]. The solution for circular cylinders is utilised in the present work. The far field form of the scattered solution is of particular relevance for the present study. For a plane incident wave the scattered far field consists of a finite number of plane waves. Let the row lie on the x-axis with adjacent scatterers spaced, centre to centre, by s, and the incident wave, ϕ_I, propagating at an angle ψ with respect to the positive x-axis, i.e. a wave of the form

$$\phi_I(x, y : \psi) = e^{ik(\beta x + \alpha y)}.$$

where $\alpha = \sin(\psi)$ and $\beta = \cos(\psi)$. The directions of the scattered waves, and hence their number, are determined by the real solutions ψ_m of

$$\psi_m = \arccos(\beta_m), \quad \text{where} \quad \beta_m = \beta + \frac{2m\pi}{ks} \quad \text{for } m \in \mathbb{Z}. \tag{1}$$

The set of integers for which real solutions of equation (1) exist is denoted $\mathcal{M}$. The far field is therefore expressed as

$$\phi(x, y) \sim \phi_I(x, y) + \sum_{m \in \mathcal{M}} a_{m\pm} e^{ik(\beta_m x \pm \alpha_m y)} \qquad (y \to \pm\infty),$$

where $\alpha_m = \sin(\psi_m)$. The elements of the set $\{\psi_m : m \in \mathcal{M}\}$ are referred to as the scattering angles. Note that $\psi_0 \equiv \psi$ so that $0 \in \mathcal{M}$. Any angle ψ_m ($m \in \mathcal{M}$) will generate the same set of scattering angles, and hence the same far field form. This property allows wave interactions between rows with the same in-row spacing to be calculated in a straightforward manner. Furthermore, the size of the set $\mathcal{M}$, M say, increases as the (non-dimensional) in-row spacing ks increases, and can change as the angle ψ is varied.

For small acoustically-soft circular cylinders the scattered amplitudes $a_{m\pm}(\psi)$ are

$$a_{m\pm} = \frac{-2}{ks\mathcal{K}\beta_m}, \quad \mathcal{K} = H_0(ka) - 1 - \frac{2i}{\pi}\left(\log\left(\frac{ks}{4\pi}\right) + C\right) + \sum_{n=1}^{\infty}\left\{\frac{2}{ks\beta_n} + \frac{2}{ks\beta_{-n}} + \frac{2i}{n\pi}\right\},$$

where H_0 is the Hankel function of the first kind order zero and $C \approx 0.5772$ is Euler's constant. The scattered field is, as expected, symmetric with respect to the x-axis. Note that the above expression for $a_{m\pm}$ is undefined if $\beta_m = 0$, i.e. $\psi_m = 0$ or π. In this situation the solution method must be modified (see e.g. Bennetts [1]). However, the extension is not required for the analysis in the current investigation, and these isolated points will simply be avoided.

2.2 A recursive solution method for multiple rows

Consider now a full array, composed of a large number of identical rows. A finite number of propagating waves are excited between each pair of adjacent rows. The waves travel in directions

defined by the scattering angles generated when the rows are in isolation, i.e. $\{\psi_m : m \in \mathcal{M}\}$. However, wave interactions between rows also involve an infinite, countable set of evanescent waves that decay exponentially away from each of the rows. The decay rate of the evanescent waves are defined by the imaginary solutions of equation (1).

A wide-spacing approximation, in which only interactions between propagating waves are considered between rows, has been applied to electromagnetic waves by McPhedran et al. [5] and to water waves by Peter & Meylan [6]. The wide-spacing approximation will also be adopted here, although it is acknowledged that in certain situations evanescent waves can have a non-negligible effect on wave interactions.

Let the rows be counted according to the point they intersect the y-axis, and suppose that row i lies on the line $y = y_i$. The wide-spacing approximation of the wave-field between rows i and $i + 1$ is

$$\phi(x, y) \approx \sum_{m \in \mathcal{M}} r_{m,i} e^{ik(\beta_m x + \alpha_m(y - \hat{y}_i))} + l_{m,i} e^{ik(\beta_m x - \alpha_m(y - \hat{y}_i))} \quad (y_i < y < y_{i+1}), \tag{2}$$

where $r_{m,i}$ and $l_{m,i}$ are the amplitudes of the upward- and downward- (with respect to the y-axis) travelling waves. The waves have been normalised to the mid-point between the rows, i.e. $\hat{y}_i = (y_i + y_{i+1})/2$. The interval $y \in (\hat{y}_{i-1}, \hat{y}_i)$, which contains a single row, will be termed the ith cell.

The time-averaged energy flux over a contour of constant y is proportional to

$$E(\phi, y) = \sum_{m \in \mathcal{M}} \alpha_m \left(|r_{m,i}|^2 - |l_{m,i}|^2 \right) \quad (y_i < y < y_{i+1}), \tag{3}$$

where the constant of proportionality depends on the physical context. In particular, the direction of energy flux, with respect to the y-axis, is deduced from the sign of E.

It is convenient to introduce matrix and vector notation at this point. Therefore, expression (2) is recast as

$$\phi(x, y) \approx e^{ik\beta x} \left(e^{ik\alpha(y - \hat{y}_i)} \mathbf{r}_i + e^{-ik\alpha(y - \hat{y}_i)} \mathbf{l}_i \right),$$

using the following notation for the size $M \times M$ diagonal matrices

$$e^{ik\beta x} = \text{diag}\{e^{ik\beta_m x} : m \in \mathcal{M}\} \quad \text{and} \quad e^{\pm ik\alpha y} = \text{diag}\{e^{\pm ik\alpha_m y} : m \in \mathcal{M}\},$$

and for the length M vectors

$$\mathbf{r}_i = \text{vec}\{r_{m,i} : m \in \mathcal{M}\} \quad \text{and} \quad \mathbf{l}_i = \text{vec}\{l_{m,i} : m \in \mathcal{M}\}.$$

The scattering properties of the cells will be expressed in terms of reflection and transmission matrices. For the individual rows the reflection and transmission matrices are denoted $R_i^{(\pm)}$ and $T_i^{(\pm)}$, respectively. These matrices are defined via

$$\mathbf{l}_{i-1} = R_i^{(-)} \mathbf{r}_{i-1} + T_i^{(+)} \mathbf{l}_i, \quad \text{and} \quad \mathbf{r}_i = T_i^{(-)} \mathbf{r}_{i-1} + R_i^{(+)} \mathbf{l}_i.$$

From § 2.1, the entries of the scattering matrices are

$$\{R_i^{(-)}\}_{p,q} = \frac{-2e^{-ik(\alpha_p + \alpha_q)\hat{y}_{i-1}}}{ks\mathcal{K}\beta_p}, \quad \{T_i^{(-)}\}_{p,q} = \frac{(\delta_{p,q} ks\mathcal{K}\beta_p - 2)e^{ik(\alpha_p \hat{y}_i - \alpha_q \hat{y}_{i-1})}}{ks\mathcal{K}\beta_p}, \tag{4a}$$

$$\{R_i^{(+)}\}_{p,q} = \frac{-2e^{ik(\alpha_p + \alpha_q)\hat{y}_i}}{ks\mathcal{K}\beta_p} \quad \text{and} \quad \{T_i^{(+)}\}_{p,q} = \frac{(\delta_{p,q}ks\mathcal{K}\beta_p - 2)e^{-ik(\alpha_p\hat{y}_{i-1} - \alpha_q\hat{y}_i)}}{ks\mathcal{K}\beta_p}, \quad (4b)$$

where $\delta_{p,q}$ is the Kronecker delta.

Similarly, the reflection and transmission matrices for the stack of cells i to j $(i < j)$ are denoted $R_{i,j}^{(\pm)}$ and $T_{i,j}^{(\pm)}$, respectively, and are defined via the expressions

$$\mathbf{l}_{i-1} = R_{i,j}^{(-)}\mathbf{r}_{i-1} + T_{i,j}^{(+)}\mathbf{l}_j, \quad \text{and} \quad \mathbf{r}_j = T_{i,j}^{(-)}\mathbf{r}_{i-1} + R_{i,j}^{(+)}\mathbf{l}_j.$$

Suppose that these matrices are known. Reflection and transmission matrices when a $(j+1)^{\text{th}}$ cell is added to the top of the stack can be calculated using the identities

$$R_{i,j+1}^{(-)} = R_{i,j}^{(-)} + T_{i,j}^{(+)}\text{inv}\{I - R_{j+1}^{(-)}R_{i,j}^{(+)}\}R_{j+1}^{(-)}T_{i,j}^{(-)}, \quad (5a)$$

$$T_{i,j+1}^{(+)} = T_{i,j}^{(+)}\text{inv}\{I - R_{j+1}^{(-)}R_{i,j}^{(+)}\}T_{j+1}^{(+)}, \quad (5b)$$

$$R_{i,j+1}^{(+)} = R_{j+1}^{(+)} + T_{j+1}^{(-)}\text{inv}\{I - R_{i,j}^{(+)}R_{j+1}^{(-)}\}R_{i,j}^{(+)}T_{j+1}^{(+)}, \quad (5c)$$

$$\text{and} \quad T_{i,j+1}^{(-)} = T_{j+1}^{(-)}\text{inv}\{I - R_{i,j}^{(+)}R_{j+1}^{(-)}\}T_{i,j}^{(-)}, \quad (5d)$$

where I is the identity matrix of size $M \times M$. An analogous expression is possible for the reflection and transmission matrices if, instead, cell $i - 1$ is added to the bottom of the stack, i.e. $R_{i-1,j}$ and $T_{i-1,j}$.

Scattering matrices can now be obtained for cells i to j, by starting with the scattering matrices for the bottommost cell i, and using identities (5) recursively to find $R_{i,n}$ and $T_{i,n}$ $(i < n \leq j)$, until the topmost cell j is reached. Alternatively, it is possible to start with the topmost cell and add cells to the bottom of the stack, using an analogue of identities (5) to find $R_{n,j}$ and $T_{n,j}$ $(i \leq n < j)$, until the bottommost cell is reached. Both methods are required to recover the set of amplitudes within the stack, via the identities

$$\mathbf{r}_n = \text{inv}\left(I - R_{i,n}^{(+)}R_{n+1,j}^{(-)}\right)\left(T_{i,n}^{(-)}\mathbf{r}_{i-1} + R_{i,n}^{(+)}T_{n+1,j}^{(+)}\mathbf{l}_j\right),$$

$$\text{and} \quad \mathbf{l}_n = \text{inv}\left(I - R_{n+1,j}^{(-)}R_{i,n}^{(+)}\right)\left(R_{n+1,j}^{(-)}T_{i,n}^{(-)}\mathbf{r}_{i-1} + T_{n+1,j}^{(+)}\mathbf{l}_j\right),$$

for $i \leq n < j$, where $\mathbf{r}_{i-1}$ and $\mathbf{l}_j$ denote the amplitudes of the waves incident on the stack from the bottom and top, respectively. The amplitudes of the waves scattered by the stack, $\mathbf{l}_{i-1}$ and $\mathbf{r}_j$, are recovered using the reflection and transmission matrices for the entire stack, via

$$\mathbf{l}_{i-1} = R_{i,j}^{(-)}\mathbf{r}_{i-1} + T_{i,j}^{(+)}\mathbf{l}_j, \quad \text{and} \quad \mathbf{r}_j = T_{i,j}^{(-)}\mathbf{r}_{i-1} + R_{i,j}^{(+)}\mathbf{l}_j.$$

2.3 Periodic problem

If the spacing of the rows in the array is a constant, d say, the scattering matrices for the individual cells, defined in equation (4), are identical. The subscripts that identify the matrices to a particular cell will thus be dropped, i.e. $R^{(\pm)} \equiv R_i^{(\pm)}$ and $T^{(\pm)} \equiv T_i^{(\pm)}$ for all i. Without loss of generality, the row locations are set as $y_n = nd$.

In the periodic setting, the wave modes supported by the array are determined from the scattering properties of a single cell. A transfer matrix method is used here. Let P be the transfer matrix that relates amplitudes on either side of a cell, i.e.

$$\begin{pmatrix} \mathbf{r}_{i+1} \\ \mathbf{l}_{i+1} \end{pmatrix} = P \begin{pmatrix} \mathbf{r}_i \\ \mathbf{l}_i \end{pmatrix}. \quad (7)$$

The transfer matrix is calculated from the reflection and transmission matrices via

$$P = \begin{pmatrix} T^{(-)} - R^{(+)}\text{inv}(T^{(+)})R^{(-)} & R^{(+)}\text{inv}(T^{(+)}) \\ -\text{inv}(T^{(+)})R^{(-)} & \text{inv}(T^{(+)}) \end{pmatrix}. \tag{8}$$

It follows from equation (7) that amplitudes in any locations in the array are related to one another through the transfer matrix, with

$$\begin{pmatrix} \mathbf{r}_j \\ \mathbf{l}_j \end{pmatrix} = P^{j-i} \begin{pmatrix} \mathbf{r}_i \\ \mathbf{l}_i \end{pmatrix}. \tag{9}$$

A diagonalisation of the transfer matrix is used to interpret relation (9). It can be shown that the eigenvalues of the transfer matrix appear in reciprocal and conjugate pairs. Therefore the diagonalisation has the form $P = X e^{iK} X^{-1}$, where

$$X = [\mathbf{x}_{1+}, \dots \mathbf{x}_{M+}, \mathbf{x}_{1-}, \dots \mathbf{x}_{M-}] \quad \text{and} \quad e^{iK} = \text{diag}\{e^{iK_1}, \dots e^{iK_M}, e^{-iK_1}, \dots e^{-iK_M}\}. \tag{10}$$

The quantities $\pm K_m$ are array wave numbers that determine how their corresponding amplitudes $\mathbf{x}_{m\pm}$ vary through the array. The local wave number k still controls the wavelengths in the intervals of free space between adjacent rows. The real parts of $\pm K_m$ produce phase changes. Note that the real parts are only defined up to an integer multiple of 2π. The imaginary parts of $\pm K_m$ induce exponential attenuation. The energy flux for a particular mode, $E = E_{m\pm}$ say, can be obtained by using the entries of the relevant vector of amplitudes, $\mathbf{x}_{m\pm}$, in the right-hand side of equation (3). Modes appearing in plus-minus pairs simply indicates that for every mode propagating and/or attenuating from bottom to top of the array, there is an equivalent mode that propagates and/or attenuates from top to bottom. The pairs $\mathbf{x}_{m\pm}$ are therefore related via

$$\mathbf{x}_{m\mp} = \mathcal{I}\mathbf{x}_{m\pm} \quad (m = 1, \dots, M), \quad \text{where} \quad \mathcal{I} = \begin{pmatrix} 0 & I \\ I & 0 \end{pmatrix}.$$

The entries of the transfer matrix, and hence the properties of the array, vary with the (non-dimensional) row spacing kd. Porter & Porter [7] numerically studied the paths of the eigenvalues of the transfer matrix in the complex plane versus kd, for a related water-wave problem. Their findings are representative of the current problem and are briefly summarised here. The eigenvalues typically traverse the unit circle, i.e. $K_m \in \mathbb{R}$ for $m = 1, \dots, M$. The corresponding modes do not attenuate through the array. However, as a pair of eigenvalues approach one another they temporarily depart the unit circle. One eigenvalue moves inside the unit circle and one outside. The imaginary component of the wave numbers induces attenuation of the corresponding modes. After this brief departure the eigenvalues rejoin the unit circle and continue on their original paths.

When only a single wave direction exists ($M = 1$) there are two eigenvalues, $e^{\pm iK_1}$. The only point at which these eigenvalues may meet is on the real axis. When they depart the unit circle, reciprocity restricts the eigenvalues to the real axis, i.e. $\pm K_1 \in i\mathbb{R}$ or $\pm K_1 \in \pi + i\mathbb{R}$. The wave numbers $\pm K_1$ are therefore only capable of producing a phase change or a change in magnitude. However, when more than one wave direction exists ($M > 1$), eigenvalues may meet on the unit circle away from the real axis. Note that an identical eigenvalue interaction will occur simultaneously in the top and bottom halves of the complex plane. When the eigenvalues depart the unit circle they are not bound to the real axis. The wave numbers K_m may, hence, possess a real and an imaginary part, in which case they produce a phase change and a change in magnitude. The intervals over which eigenvalues depart the unit circle are located near the points $\alpha_p + \alpha_q = 2\pi/kd$ ($p, q \in \mathcal{M}$), where $p = q = 1$ can be identified as classical Bragg resonance.

2.4 Disordered problem and approximation via random sampling

Disorder in the separation of the rows is introduced through the random parameters $\varepsilon_n \in (-0.5, 0.5)$, with the location of row n shifted to $y_n = (n + \varepsilon_n)d$. Values of ε_n for all rows in the array are randomly selected from a prescribed distribution. Calculations presented in this study use a uniform distribution of width $\varepsilon \in [0, 1)$, i.e. $\varepsilon_n \in \mathcal{U}(-\varepsilon/2, \varepsilon/2)$. The case $\varepsilon = 0$ reproduces the periodic problem.

The effect of disorder on the modes supported by the array will be investigated using two distinct approaches. Firstly, an approach based on localisation theory. It is expected that disorder will induce exponential attenuation. In problems involving only a single wave direction the logarithm of transmitted energy is self-averaging, and hence the modes excited in almost all realisations of sufficiently large stacks will display the same attenuation rate (Berry & Klein [2]). The expected rate of attenuation can therefore be estimated numerically as the mean attenuation rate of a sample of individual wave fields for randomly generated realisations of large finite stacks. However, in problems involving multiple wave directions, individual wave fields are composed of more than one mode, each with a different attenuation rate. A more complete numerical method is proposed below to capture the different attenuation rates. The associated phase changes are also considered as part of the method.

The second approach is based on effective media theory. The effective or coherent wave modes are extracted from the ensemble average wave field, with respect to all possible realisations of the disorder. Maurel et al. [4] provide illustrative graphical examples of coherent waves in one-dimensional problems. They also describe how a coherent wave, composed of only a single mode, can be estimated numerically. As in the localisation approach, the method relies on calculating individual wave fields for a sample of randomly generated realisations of large finite stacks. The numerical method is extended here to allow for effective wave fields composed of multiple modes.

The two approaches may be loosely summarised as (i) extract the required information from the individual wave fields and then average, and (ii) average the individual wave fields and then extract the required information. The difficulty in extending the numerical methods to implement either of the two approaches is best described by returning to the periodic problem, where no averaging is required. A wave field is forced by an incident wave, which, without loss of generality, originates at the far field beneath the stack $(y \to -\infty)$. For simplicity, consider a case in which all of the array wave numbers, $\pm K_m$, have an imaginary component, so that the wave field must attenuate through the stack. Numerical calculations require the stack to be of finite length, consisting of rows 1 to $N + 1$ say. Let N be large enough to ensure the wave field will attenuate sufficiently by the end of the stack that the wave reflected by that boundary is negligible. The wave amplitudes within the stack are therefore

$$\begin{pmatrix} \mathbf{r}_n \\ \mathbf{l}_n \end{pmatrix} = \sum_{m=1}^{M} c_m \mathrm{e}^{\mathrm{i}K_m n} \mathbf{x}_{m+} \qquad (n = 1, \ldots, N), \tag{11}$$

for some constants c_m $(m = 1, \ldots, M)$. The primary problem is now to obtain the array wave numbers, K_m, from the amplitudes on the left-hand side of equation (11). If the problem is one dimensional, i.e. $M = 1$, the single mode is automatically uncoupled, and the wave number can be recovered using a simple linear regression. However, if multiple waves exist, i.e. $M > 1$, the various modes are coupled in the amplitudes. The most slowly attenuating mode will eventually dominate, and can in theory be estimated by cutting off a band of the bottommost rows. However, the number of rows cut off is problem dependent and is therefore

difficult to implement numerically. It also does not give information on the spectrum of array wave numbers.

With the simple example above acting as motivation, attention now returns to the disordered problem. For each randomly generated realisation of the stack, a set of $2M$ linearly independent incident waves $(\mathbf{r}_0, \mathbf{l}_{N+1}) = (\mathbf{r}_{0,m\pm}, \mathbf{l}_{N+1,m\pm})$ $(m = 1, \ldots, M)$ are used, where

$$[\mathbf{r}_{0,1-}, \ldots, \mathbf{r}_{0,M-}] = [\mathbf{l}_{N+1,1+}, \ldots, \mathbf{l}_{N+1,M+}] = I,$$

$$\text{and} \quad [\mathbf{r}_{0,1+}, \ldots, \mathbf{r}_{0,M+}] = [\mathbf{l}_{N+1,1-}, \ldots, \mathbf{l}_{N+1,M-}] = 0.$$

The corresponding amplitudes within the stack are denoted $(\mathbf{r}_n, \mathbf{l}_n) = (\mathbf{r}_{n,m\pm}, \mathbf{l}_{n,m\pm})$ $(n = 1, \ldots, N)$. To follow the localisation approach, ansatzes of the form

$$\begin{pmatrix} \mathbf{r}_{n,m-} \\ \mathbf{l}_{n,m-} \end{pmatrix} = \sum_{j=1}^{2M} c_{j,m-} \mathrm{e}^{\mathrm{i}Q_j^{(1)} n} \mathbf{v}_j^{(1)} \quad \text{and} \quad \begin{pmatrix} \mathbf{r}_{N+1-n,m+} \\ \mathbf{l}_{N+1-n,m+} \end{pmatrix} = \sum_{j=1}^{2M} c_{j,m+} \mathrm{e}^{-\mathrm{i}Q_j^{(1)} n} \mathbf{v}_j^{(1)} \qquad (12)$$

for $n = 1, \ldots, N$ and $m = 1, \ldots, M$, are assumed. The quantities Q_j are array wave numbers, and $\mathbf{v}_j$ are the corresponding vectors of amplitudes. The subscript (l) is used, when necessary, on these quantities to distinguish them from the corresponding quantities obtained from effective media theory. For the uniform distributions considered in this work, Q_j and $\mathbf{v}_j$ are functions of ε, as well as of the properties of the rows and incident wave field. It is expected that symmetry, in terms of the distribution of disorder, will allow the wave numbers to be ordered such that $Q_j \approx Q_{M+j}$ $(j = 1, \ldots, M)$, and, similarly, the amplitude vectors such that $\mathbf{v}_j \approx \mathcal{I}\mathbf{v}_{M+j}$.

The wave fields produced by the independent incident waves are used to separate the different modes. The two components of equation (12) are combined to produce the matrix expression $A_n = V\mathrm{e}^{\mathrm{i}Q^{(1)}n}\mathrm{inv}(V)$, where $V = [\mathbf{v}_1, \ldots, \mathbf{v}_{2M}]$, $\mathrm{e}^{\mathrm{i}Qn} = \mathrm{diag}\{\mathrm{e}^{\mathrm{i}Q_1 n}, \ldots, \mathrm{e}^{\mathrm{i}Q_{2M} n}\}$ and $A_n = A_{n,N+1}\mathrm{inv}(A_{0,N+1-n})$, where

$$A_{p,q} = \begin{pmatrix} \mathbf{r}_{p,1-}, & \ldots, & \mathbf{r}_{p,M-}, & \mathbf{r}_{q,1+}, & \ldots, & \mathbf{r}_{q,M+} \\ \mathbf{l}_{p,1-}, & \ldots, & \mathbf{l}_{p,M-}, & \mathbf{l}_{q,1+}, & \ldots, & \mathbf{l}_{q,M+} \end{pmatrix}.$$

Linear regression is applied to the eigenvalues of matrices A_n $(n = 1, \ldots, N)$ to produce the array wave numbers Q_j $(j = 1, \ldots, 2M)$. The final approximation is obtained by averaging the wave numbers Q_j over a large number of simulations.

Although the above algorithm is seemingly straightforward, the combination of exponential growth and decay, and of different rates of the growth/decay create numerical difficulties. The structure of the matrix system adopted here is motivated by numerical stability. Using the symmetry of the eigenvalues and eigenvectors would undoubtedly improve stability further, but it is unclear how this may be implemented.

The ansatzes contained in equation (12) are not applied for the effective media approach. Equivalent ansatzes are instead assumed for the ensemble average of the amplitudes over the different realisations. The ansatzes are expressed as:

$$\begin{pmatrix} \langle\langle \mathbf{r}_{n,m-} \rangle\rangle \\ \langle\langle \mathbf{l}_{n,m-} \rangle\rangle \end{pmatrix} = \sum_{j=1}^{2M} c_{j,m-} \mathrm{e}^{\mathrm{i}Q_j^{(\mathrm{e})} n} \mathbf{v}_j^{(\mathrm{e})}; \quad \begin{pmatrix} \langle\langle \mathbf{r}_{N+1-n,m+} \rangle\rangle \\ \langle\langle \mathbf{l}_{N+1-n,m+} \rangle\rangle \end{pmatrix} = \sum_{j=1}^{2M} c_{j,m+} \mathrm{e}^{-\mathrm{i}Q_j^{(\mathrm{e})} n} \mathbf{v}_j^{(\mathrm{e})}, \qquad (13)$$

for $n = 1, \ldots, N$ and $m = 1, \ldots, M$, where the double angled brackets $\langle\langle \cdot \rangle\rangle$ denote the ensemble average with respect to all realisations of the random disorder. The ensemble averages of the

amplitudes are approximated as the mean values of a large number of simulations. The method of decomposing the average wave field into the spectrum of modes follows the algorithm used for the individual simulations in the localisation approach.

To conclude, the quantities averaged are: the modal wave numbers in the localisation approach; and the amplitudes of waves between adjacent rows in the effective media approach.

3 Numerical results: analysis using random sampling

3.1 Single wave direction ($M = 1$)

Figure 1 shows examples of an individual wave field and a coherent wave, which have been decomposed into the modes supported by the array. The problem under consideration has in-row spacing $ks = \pi$, mean row spacing $kd = 2.5\pi$, and propagating waves travelling only in the direction perpendicular to the rows, i.e. an angle $\pi/2$ with respect to the x-axis. The underlying periodic medium has array wave numbers $\pm K_1 = \pm 0.4214\pi$, which defines a pass-band state. The level of disorder in the row spacing is set at $\varepsilon = 10^{-0.5}$.

The wave fields are evaluated at the mid-points between the rows of the underlying periodic medium, i.e. $\hat{y}_n = nd$ for $n = 1, \ldots, N$. The natural logarithm of the wave fields are shown. These are the signals used to extract estimates of the array wave numbers Q_1 and $Q_2 \approx -Q_1$. The top panels show the imaginary parts of the wave fields and the bottom panels show the negative of the real part of the wave fields. These quantities correspond, respectively, to the real and imaginary parts of the array wave numbers, i.e. the phase changes and attenuation rate.
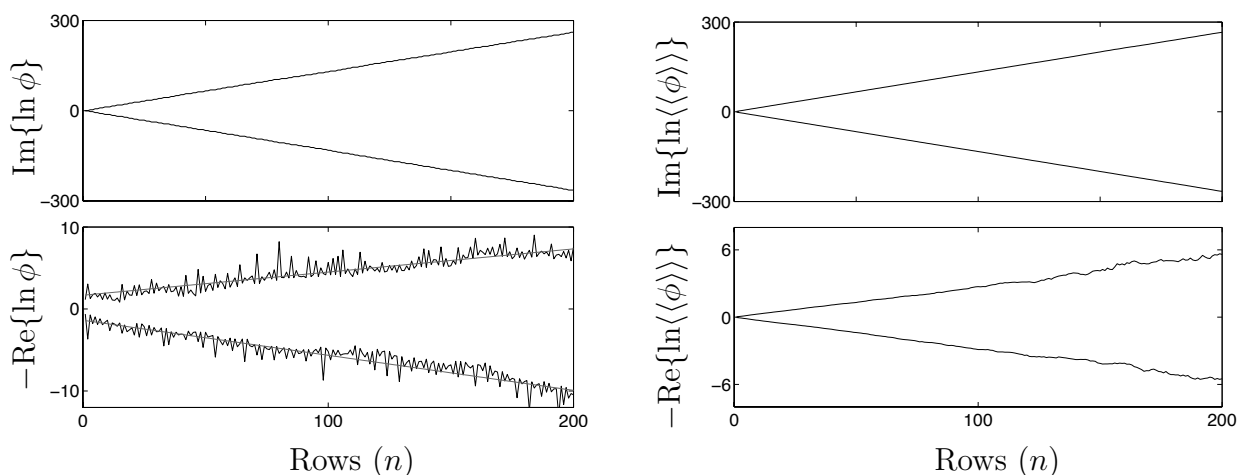

Figure 1: Examples of an individual wave field (left-hand panels) and a coherent wave field (right) for a single-wave problem, and disorder level $\varepsilon = 10^{-0.5}$. The black curves in the left-hand panels are the spectral components of the wave field for a single realisation of the disorder. The grey curves on the bottom left-hand panel are the straight-line fits of the attenuation rates. The curves in the right-hand panels are the spectral components of the coherent wave.

The left-hand panels of figure 1 show wave fields for a single randomly generated realisation of the disorder. Variations in the distance between the rows produce noise in the individual wave fields. The noise is clearly visible in the attenuation of the wave fields shown in the bottom panel. The straight-line fits used to extract the imaginary parts of the array wave numbers are

hence also included. However, the noise is not evident on the scale of the phase changes shown in the top panel, which are dominated by the underlying periodic structure.

The values of the array wave numbers obtained from the simulation shown in left-hand panels of figure 1 are $Q_1 \approx -0.4237\pi + 0.028\mathrm{i}$ and $Q_2 \approx 0.4163\pi - 0.043\mathrm{i}$. A large number of these wave numbers are averaged to produce the localisation approximation of the array wave numbers for the random medium. In comparison, the wave fields themselves are averaged to find the effective media approximation of the wave numbers. An example of an effective wave field is shown in the right-hand panels of figure 1. The wave field is calculated as the average of 5×10^3 randomly generated simulations. The coherent wave field matches ansatzes (13) to the extent that overlaying the straight-line fits on the panels is unnecessary. The noise visible from approximately 120 rows onwards in the bottom panel is attributed to accumulation of rounding errors in the exponentially small values produced by attenuation.

Approximations, obtained from the localisation and effective media approaches, of the array wave number Q_1, with positive energy flux and/or attenuating in the positive y-direction, are compared in figure 2. The wave numbers are shown as functions of the disorder parameter ε. The real and imaginary parts of Q_1, i.e. the phase changes and attenuation rates, are shown in the top and bottom panels, respectively. The results shown in the left-hand panels are for the array considered in figure 1, for which the underlying periodic problem is in a pass-band state. For the results shown in the right-hand panels the mean row spacing is changed to $kd = 4.1\pi$. The array wave numbers for the underlying periodic problem in this case are $\pm K_1 \approx \pm 0.230\mathrm{i}$, which defines a stop-gap state.

Additional data on the ensemble used in the localisation approach for selected values of disorder level are provided in the panels. The bars on the bottom left-hand panel denote one standard deviation confidence intervals of the attenuation rates. The bar graphs on the top left-hand panel represent the logarithmically scaled distribution of the phase changes in the ensemble. The grey curves with pluses and crosses in the top right-hand panel are the phase changes for the amplitudes of the local waves travelling upward, i.e. $r_{m,i}$, and downward, i.e. $l_{m,i}$, respectively, when the only mode excited is that attenuating from bottom to top of the array.

The two approaches produce almost identical approximations of the attenuation rates for both problems. However, the approximations diverge from one another as the disorder decreases for the problem with the underlying pass-band state. The difference is attributed to numerical difficulties in capturing small attenuation rates using the localisation approach. Loss of accuracy in the localisation approach is indicated in the results by deviation from the linear log-log relationship between attenuation rate and disorder. (Further, note that the relative magnitude of the standard deviation to the attenuation rate increases as the attenuation rate decreases.) Accuracy is improved by increasing the number of rows in the array. For this reason $N = 750$ rows were used for the problem with the underlying pass band state, in comparison to $N = 250$ rows for the problem with the underlying stop gap state. The number of rows that may be used in practice is, however, bounded by numerical constraints. Consequently, differences in the attenuation rates predicted by the two approaches are observed close to pass-band states throughout the results presented in § 3.

For large disorder, the convergence of the effective media approach is generally slower than that of the localisation approach with respect to the ensemble size. This can be inferred from the greater noise present in the effective media approximations, which is most clear in the bottom right-hand panel. Rapid convergence of the attenuation rate with respect to ensemble size for the localisation approach is expected due to the self-averaging property referred to in

§ 2.4.

The attenuation rates for both problems settle to the same value as the magnitude of the disorder in increased. The attenuation rate predicted for large disorder is consistent with the expression derived by Berry & Klein [2] for a stack of transparent plates. This attenuation rate is $-\ln|\tau|$, where τ is the transmission coefficient for a single scatterer in the array, which, in the present setting, is a single row. The expected limit for the problems used in figure 2 is $-\ln|\tau| \approx 0.029$, and is shown by the chained curve in the bottom panels. The derivation of the limit assumes that wave interactions between adjacent scatterers range over all phases, which here requires that $\varepsilon kd \geq \pi$. The corresponding value of the disorder is $\log_{10}\varepsilon \gtrsim -0.398$ in the left-hand panels, and $\log_{10}\varepsilon \gtrsim -0.613$ in the right-hand panels. Berry & Klein [2] did not, however, consider a perturbed periodic geometry. It is noted that the predicted attenuation rates for $\varepsilon kd \geq \pi$ display small amplitude oscillations around the limit $-\ln|\tau|$.
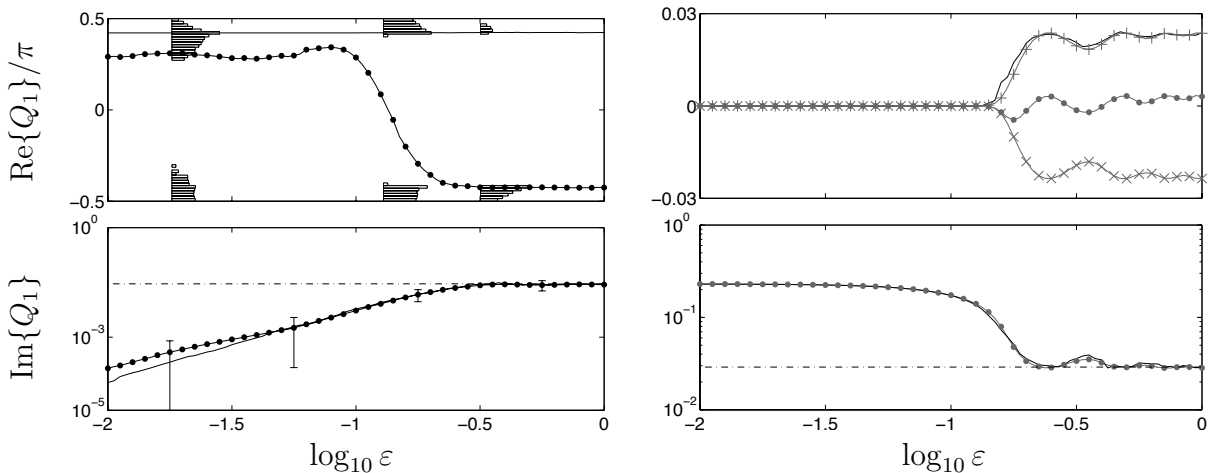

Figure 2: Comparisons of array wave numbers produced by the localisation approach (grey-dotted curves) and effective media approach (black curves), as functions of disorder level, for a single-wave problem. The underlying periodic problem is in a pass-band state (left-hand panels), and a stop-gap state (right). The distribution of the real part of the array wave numbers are superimposed on the top left-hand panel. The real parts of the array wave numbers associated to the upward and downward local waves are superimposed on the top right-hand panel. One standard deviation confidence intervals of the imaginary part of the array wave numbers are included in the bottom left-hand panel. The broken curves on the bottom panels denote the Berry & Klein [2] limit.

The top panels demonstrate that the localisation and effective media approaches do not predict the same phase changes beyond small disorder. Numerical investigations indicate that the approximation given by the localisation approach is often unrepresentative of the waves supported by the array. This assertion appears to contradict the top left-hand panel of figure 1, in which the phase changes of individual wave fields are shown to be consistent with ansatzes (12). The behaviour is partially explained with reference to the problem with the underlying stop-gap state, where the modes are automatically uncoupled in the individual simulations for all levels of disorder. The phase changes associated to the upward travelling local waves match with those of the mode it shares its attenuation rate with, i.e. Q_1, whereas the phase changes associated to the downward waves are match those of the mode that attenuates in the opposite direction, i.e. $Q_2 \approx -Q_1$. As the level of disorder is increased, the magnitude of the incoherent part of the wave fields becomes comparable to that of the coherent part. The attenuation

rate, which is a global property, is unaffected, but the phase change, which is a local property, no longer resembles one of the coherent wave modes. The curves and bar graphs in the top left-hand panel, show a case in which the phase changes of the individual wave fields transition from being dominated by the upward waves to the downward waves, as the level of disorder is increased. Unfortunately, no obvious method exists to decouple the phase changes in the individual wave fields when multiple modes are excited.

3.2 Multiple wave directions ($M \geq 2$)

For symmetric configurations of wave directions, i.e. problems in which for every non-zero β_m ($m \in \mathcal{M}$) there exists a β_j such that $\beta_j = -\beta_m$, the periodic problem possesses at least two array wave number/eigenvector pairs that are unaffected by disorder. One of the modes in each pair propagates up the array. The corresponding eigenvector contains non-zero entries only for amplitudes of local waves that travel up the array. Disorder then merely changes the phase at which these waves interact with the rows. As no reflected component will be excited, the destructive interference that causes attenuation (Berry & Klein [2]) does not occur. The second mode is simply the equivalent wave travelling down the array. Any incident wave that is not orthogonal to these modes will therefore not fully attenuate with distance through the array.

Figures 3–4 show examples of an individual wave field and a coherent wave field, decomposed into the modes supported by the array. The figures are equivalent to figure 1, but for problems involving multiple wave directions. The arrays used for figure 3 have in-row spacing $ks = \pi \sec(\pi/4)$, mean row spacing $kd = 8\pi$, and two wave directions, $\pi/2 \pm \pi/4$ with respect to the x-axis. The arrays used for figure 4 have in-row spacing $ks = 2\pi \sec(3\pi/10)$, mean row spacing $kd = 7.9\pi$, and three wave directions, $\pi/2 + 3m\pi/10$ ($m = 0, \pm 1$), with respect to the x-axis. The underlying periodic media for both problems are in pass-band states, with $\pm K_1 \approx \pm 0.343\pi$ and $\pm K_2 \approx \pm 0.498\pi$ for the two-wave problem, and $\pm K_1 \approx \pm 0.391\pi$, $\pm K_2 \approx \pm 0.124\pi$ and $\pm K_3 \approx \pm 0.338\pi$ for the three-wave problem. The row spacing disorder level is again set at $\varepsilon = 10^{-0.5}$. The coherent waves are calculated using 10^3 random realisations for the two-wave problem, and 5×10^3 random realisations for the three-wave problem. Both problems are of the symmetric type discussed at the beginning of the section. In each problem, two modes will exist that do not attenuate, and this is confirmed by the bottom panels.

The example wave fields are presented to validate use of ansatzes (12) or (13) for problems involving multiple wave directions. Note the large amount of noise in the attenuation component of the individual wave fields for the three-wave problem, shown in the bottom left-hand panel of figure 4. This is attributed to the small attenuation rates of the modes. Noise is also apparent in the corresponding coherent wave. Further, note in the corresponding phase changes that the $+/-$ pairing symmetry is broken, which is associated to the phenomenon discussed in the final paragraph of § 3.1 for the single-wave problem.

The attenuation rates predicted by the two approaches, as functions of the disorder parameter, are compared in figures 5 and 6 for problems involving two and three wave directions, respectively. For reference, the wave numbers are ordered in ascending magnitude of imaginary component. The results shown in the top left-hand panel of figure 5 are for the same array used in figure 3. The approximation of the mode with zero attenuation, $\text{Im}\{Q_1\} = 0$, is omitted for clarity. Results for a different row spacing, $kd = 7.3\pi$, are shown in the top right-hand panel. In this case, the mode with wave number Q_2 is in a stop-gap state for zero disorder. The results shown in the bottom panels are for arrays composed of the same rows as the top panels, but with scattering angles 0.1π and 0.653π, i.e. the problem is asymmetric with respect
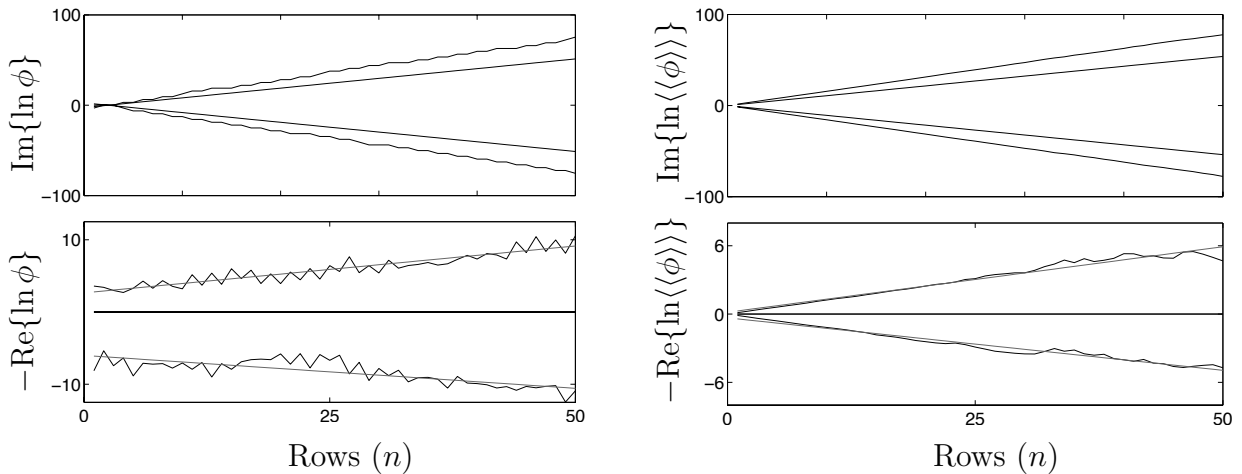
Figure 3: As in figure 1, but for a two-wave problem.
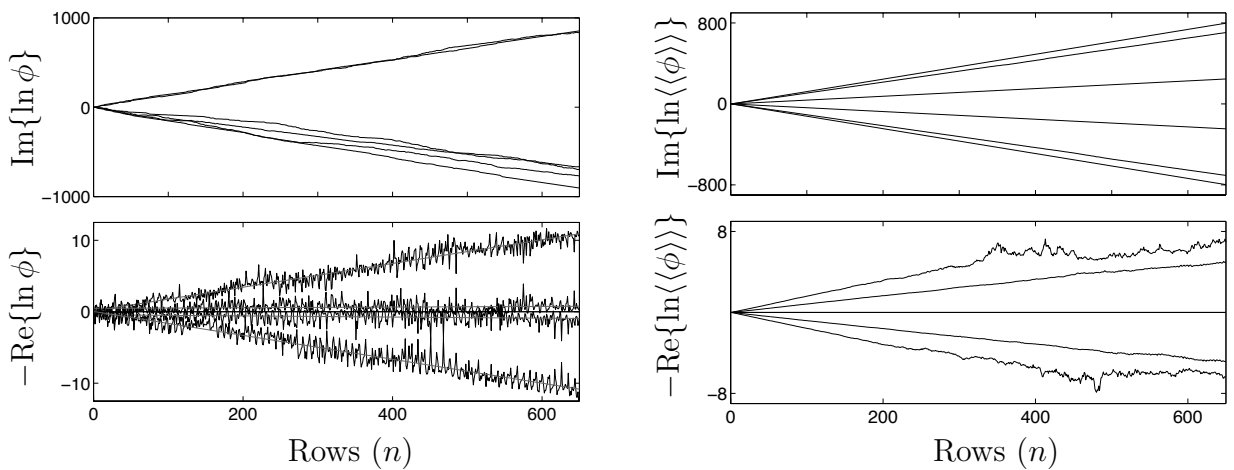

Figure 4: As in figure 1, but for a three-wave problem.

to the y-axis. Both modes therefore vary due to disorder, and approximations are presented for both. The row spacings are $kd = 8\pi$ in the bottom left-hand panel, and $kd = 7.5\pi$ in the bottom right-hand panel.

The results shown in the left-hand panels of figure 6 are for the same array used in figure 4. Results for a different row spacing, $kd = 7.5\pi$, are shown in the right-hand panels. As in figure 5, the approximation of the mode with zero attenuation, again labelled with unit subscript, is omitted. The approximations of the two remaining wave numbers, Q_2 and Q_3, are presented in the bottom and top panels, respectively. One standard deviation confidence intervals for the localisation approach are overlaid on the panels. Note that, for small attenuation rates, in three cases the lower limit of the bar becomes negative, and are hence outside the range of the ordinate axis.

The following observations are made for the symmetric two-wave problems shown in the top panels of figure 5.

(i) The attenuation rates are identical for almost all levels of disorder.

(ii) They differ for small attenuation rates, which the localisation approach is unable to capture accurately with the given numerical constraints.
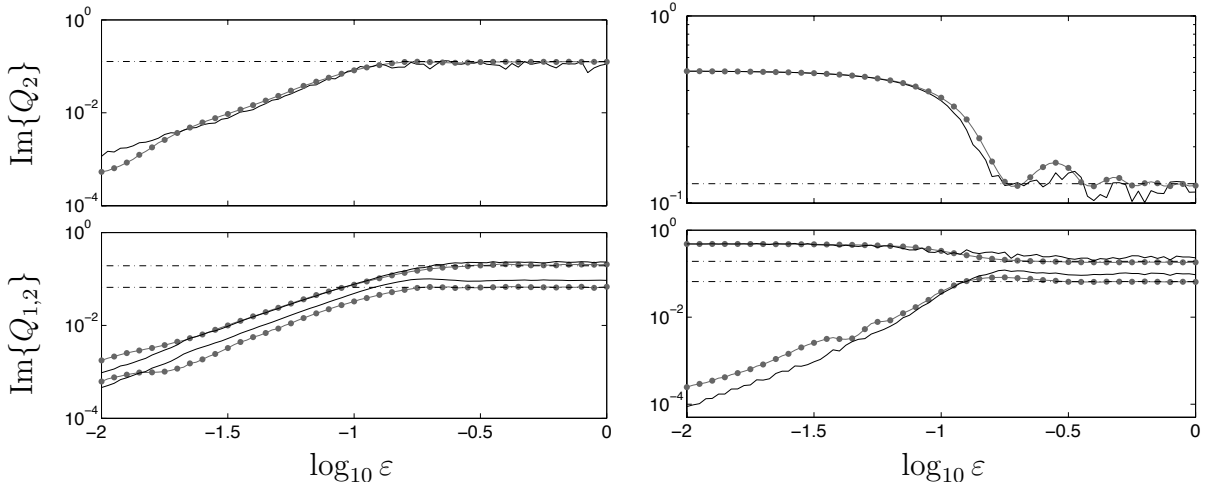
13

Figure 5: Comparisons of the imaginary parts of the array wave numbers produced by the localisation approach (grey-dotted curves) and effective media approach (black curves), as functions of disorder level, for two-wave problems. The problem is symmetric with respect to the y-axis in the top panels, and asymmetric in the bottom panels. In the symmetric case only the array wave number that varies with the disorder is shown. The broken curves are the averages of the imaginary parts of the wave numbers for $\log_{10} \varepsilon \in (-0.5, 0)$.
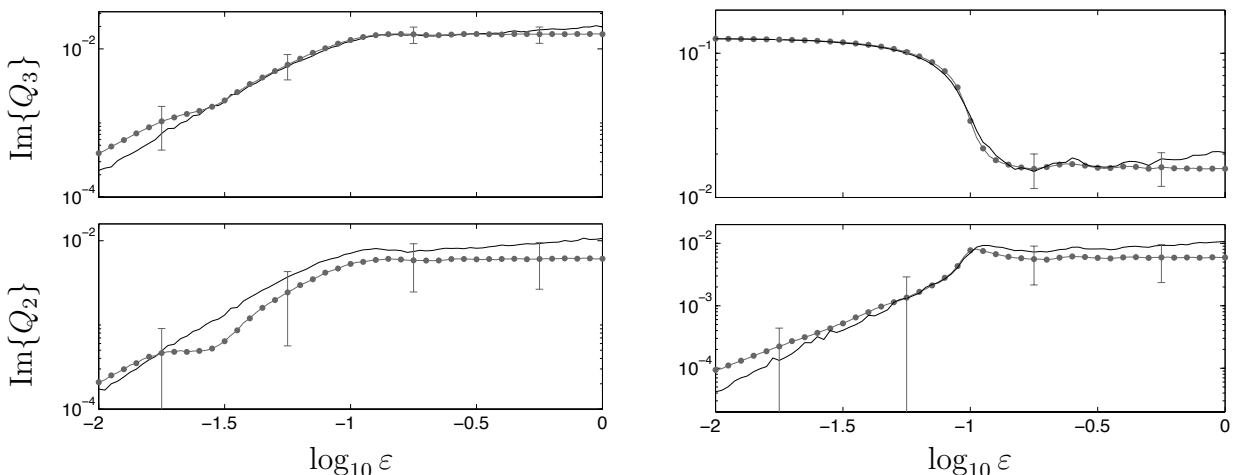

Figure 6: Comparisons of the imaginary parts of the array wave numbers produced by the localisation approach (grey-dotted curves) and effective media approach (black curves), as functions of disorder level, for three-wave problems. The problems are symmetric with respect to the y-axis, and only the array wave numbers that vary with the disorder are shown. One standard deviation confidence intervals are also shown.

(iii) The attenuation rates settle to an approximately constant value for large disorder, and the value is independent of the underlying periodic geometry.

These observations are identical to those made for the single wave direction problems. It is likely that this is due to symmetry of the two wave directions, i.e. there is only a single local wave number in the y-direction. For problems involving two or more wave directions, however, the attenuation limit for large disorder can not be obtained from the Berry & Klein [2] formula. Equality of the attenuation rates for large disorder is instead demonstrated using the mean of the approximate attenuation rates for $\log_{10} \varepsilon \in (-0.5, 0)$.

14

The different approaches also produce similar approximations of the attenuation rates for the asymmetric two-wave problems and three-wave problems. However, two fundamental differences are evident for large disorder.

(i) In the two-wave problems, the attenuation rates predicted by both approaches settle to approximately constant values. The attenuation rates predicted by the effective media approach are slightly greater than those of the localisation approach.

(ii) In the three-wave problems the attenuation rates of the effective wave modes continue to increase after the attenuation rates of the individual wave fields have settled.

The attenuation rates for large disorder are still independent of the underlying periodic medium, i.e. the row spacing. This is indicated for the two-wave problems by chained lines, which represent the mean attenuation rate predicted by the localisation approach for $\log_{10} \varepsilon \in (-0.5, 0)$. Equivalence of the approximations given by the effective media approach can also be inferred from these values.

The corresponding approximations given by the two approaches, in general, match for an interval of the disorder parameter. The interval lies above the point (if it exists) where inaccuracies become apparent in the localisation approach, and below the point where the approximations genuinely begin to differ. Inaccuracies in the localisation approach are naturally more pronounced for wave numbers with smaller imaginary values — note that these are the modes that travel for the greatest distance through the array before becoming vanishingly small. In some of the examples shown, namely Q_1 in the bottom left-hand panel of figure 5 and Q_2 in the bottom left-hand panel of figure 6, the attenuation rates do not agree for any interval of the disorder parameter. It is likely that this is caused simply by an overlap of the intervals in which inaccuracies are present in the localisation approach and where the attenuation rates genuinely differ. It is, however, difficult to prove this due to numerical limitations.

4 Coherent potential approximation

The structure of the coherent potential approximation (CPA) is closely related to that of the periodic problem considered in § 2.3. Suppose then, to begin with, that a single cell is isolated in an otherwise infinite periodic array, which is referred to as the background medium. Without loss of generality, the cell will be centred on the x-axis. The cell therefore occupies the interval $y \in (-d/2, d/2)$, where d is the row spacing in the periodic background medium. The row contained within the cell may be positioned on any contour of constant y in the interval $(-d/2, d/2)$.

Recall that modes supported by the periodic background medium have array wave numbers $\pm K_m$ ($m = 1, \ldots, M$) and corresponding amplitude vectors $\mathbf{x}_{m\pm}$. Consider one of these modes propagating (or attenuating) through the background medium, and incident on the isolated cell. If the row contained in the cell is positioned on the x-axis, the full array is periodic. The incident mode will therefore continue to propagate (or attenuate) through the cell in the same manner as through the cells in the background medium. However, if the row is not located on the x-axis, only a proportion of the mode will be transmitted by the cell, with the remaining proportion being reflected.

The interaction of any incident wave mode j ($j = 1, \ldots, M$) with the cell excites all of the other modes in reflection and transmission. Let the position of the row in the cell be $y = \varepsilon_0 d/2$,

where $\varepsilon_0 \in (-1, 1)$. The excitation of the modes is expressed using the extended transfer matrix relation

$$\sum_{m=1}^{M} \mathrm{e}^{\mathrm{i}K_m} \mathcal{T}_{m,j}(\varepsilon_0)\mathbf{x}_{m+} = P(\varepsilon_0) \left\{ \mathbf{x}_{j+} + \sum_{m=1}^{M} \mathcal{R}_{m,j}(\varepsilon_0)\mathbf{x}_{m-} \right\} \text{ for } j = 1, \ldots, M. \qquad (14)$$

The above expression assumes an incident mode from below the cell. The expression for an incident wave from above the cell is analogous. In equation (14) the quantities $\mathcal{R}_{m,j}$ and $\mathcal{T}_{m,j}$ $(m, j = 1, \ldots, M)$ are, respectively, unknown reflection and transmission coefficients. Note that these coefficients relate to the wave modes supported by the array, and are distinct from the coefficients that relate to waves supported between the rows (4). The transfer matrix $P(\varepsilon_0)$ is calculated using expression (8), where the entries of the reflection and transmission matrices, $R^{(\pm)}$ and $T^{(\pm)}$, are evaluated for $\hat{y}_{i-1} = d(1 + \varepsilon_0)/2$ and $\hat{y}_i = d(1 - \varepsilon_0)/2$.

Let reflection and transmission matrices be denoted by $\mathcal{R}$ and $\mathcal{T}$, respectively, with entries $\{\mathcal{R}\}_{m,j} = \mathcal{R}_{m,j}$ and $\{\mathcal{T}\}_{m,j} = \mathcal{T}_{m,j}$ $(m, j = 1, \ldots, M)$. Manipulations of the transfer matrix relations (14) can be used to produce the expression for the reflection matrix

$$\mathcal{R} = -\mathrm{inv}\Big(\mathrm{inv}(\mathcal{X})\mathcal{N}_{1,2} - \mathrm{inv}(\mathcal{Y})\mathcal{M}_{2,1}\Big)\Big(\mathrm{inv}(\mathcal{X})\mathcal{M}_{1,2} - \mathrm{inv}(\mathcal{Y})\mathcal{N}_{2,1}\Big), \qquad (15a)$$

and for the scaled transmission matrix $\widehat{\mathcal{T}} \equiv \mathrm{e}^{\mathrm{i}K}\mathcal{T}$,

$$\widehat{\mathcal{T}} = \mathrm{inv}\Big(\mathrm{inv}(\mathcal{N}_{1,2})\mathcal{X} - \mathrm{inv}(\mathcal{M}_{2,1})\mathcal{Y}\Big)\Big(\mathrm{inv}(\mathcal{N}_{2,1})\mathcal{M}_{1,2} - \mathrm{inv}(\mathcal{M}_{2,1})\mathcal{N}_{2,1}\Big), \qquad (15b)$$

which combines the wave numbers K_m $(m = 1, \ldots, M)$ and transmission coefficients. In the above expressions the matrices $\mathcal{M}_{i,j}$ and $\mathcal{N}_{i,j}$ $(i, j = 1, 2)$ are defined by

$$\mathcal{M}_{i,j} \equiv P_{i,i}\mathcal{X} + P_{i,j}\mathcal{Y} \quad \text{and} \quad \mathcal{N}_{i,j} \equiv P_{i,i}\mathcal{Y} + P_{i,j}\mathcal{X},$$

and the following block matrix notation is used for the transfer matrix, P, and matrix of eigenvectors, X, defined in equation (10):

$$P = \begin{pmatrix} P_{1,1} & P_{1,2} \\ P_{2,1} & P_{2,2} \end{pmatrix} \quad \text{and} \quad X = \begin{pmatrix} \mathcal{X} & \mathcal{Y} \\ \mathcal{Y} & \mathcal{X} \end{pmatrix}.$$

The reflection and transmission coefficients $\mathcal{R}_{m,j}$ and $\mathcal{T}_{m,j}$ $(m, j = 1, \ldots, M)$ are therefore obtained using equations (15) for a given value of ε_0 from the known properties of the periodic background medium.

The problem is now altered by replacing the periodic background medium with a randomly disordered background medium. It is assumed that the random medium supports modes with array wave numbers $\pm Q_m$ $(m = 1, \ldots, M)$ and corresponding amplitude vectors $\mathbf{v}_{m\pm}$. The form of the transfer matrix relation (14) and expressions for the reflection and transmission matrices (15) are still valid. However, the known wave numbers K_m and amplitude vectors $\mathbf{x}_{m\pm}$, are replaced by unknowns Q_m and $\mathbf{v}_{m\pm}$, respectively. The problem is now (i) non-linear, and, moreover, (ii) for any given realisation the number of unknowns exceeds the number of equations available. Note that the reflection and transmission coefficients $\mathcal{R}_{m,j}$ and $\mathcal{T}_{m,j}$ will have different values for the random background medium, although the same notation is retained.

The second issue is resolved by taking ensemble averages of the reflection and transmission coefficients $\mathcal{R}_{m,j}$ and $\mathcal{T}_{m,j}$ over all possible realisations within the cell, and invoking a CPA-style

hypothesis. It is assumed that if the distribution of the position of the row in the isolated cell is identical to that of the rows in the cells of the background medium, then, on average, the cell is transparent with respect to the background medium. The CPA is expressed in terms of the reflection and transmission coefficients as

$$\langle \mathcal{R}_{m,j} \rangle = 0 \quad \text{and} \quad \langle \mathcal{T}_{m,j} \rangle = \begin{cases} 1 & (m = j), \\ 0 & (m \neq j), \end{cases} \quad \text{for} \quad m, j = 1, \dots, M.$$

Angled brackets $\langle \cdot \rangle$ are used here to denote the ensemble average over all possible positions of the row in the cell, i.e. for the uniform distribution

$$\langle \cdot \rangle \equiv \int_{-\epsilon/2}^{\epsilon/2} \cdot (\varepsilon_0) \, \mathrm{d}\varepsilon_0.$$

The remaining non-linear problem is solved numerically. A Nelder-Mead minimisation routine (`fminsearch` in the MatLab Optimization toolbox) is employed to calculate the $2M^2$ entries contained in matrices $\mathcal{X}$ and $\mathcal{Y}$ from the $2M(M-1)$ conditions of the CPA,

$$\langle \mathcal{R}_{m,j} \rangle = 0 \quad (m, j = 1, \dots, M) \quad \text{and} \quad \langle \mathrm{e}^{\mathrm{i}Q_m} \mathcal{T}_{m,j} \rangle = 0 \quad (m, j = 1, \dots, M; m \neq j),$$

using the relevant entries of expressions (15), and M normalisation conditions to ensure uniqueness of the eigenvectors. A penalty term is also included to force the minimisation routine to seek modes with non-negative energy flux. The wave numbers Q_m are subsequently found by using the calculated values of $\mathcal{X}$ and $\mathcal{Y}$ in equation (15b) to obtain the diagonal elements of $\widehat{\mathcal{T}}$, and applying the final M CPA conditions

$$\langle \mathrm{e}^{\mathrm{i}Q_m} \mathcal{T}_{m,m} \rangle = \mathrm{e}^{\mathrm{i}Q_m} \quad (m = 1, \dots, M).$$

CPA results presented in § 5 are calculated using a homotopy method. The level of disorder is increased in steps, with the numerical solution for the previous step used as the initial guess for the minimisation routine. The known solution of the underlying period medium is used as an initial guess for the first step. Residual errors of the numerical solutions are generally small, and the convergence of the effective wave modes is satisfactory. However, it is difficult to drive the error to zero by decreasing the step size, and consequently prove that a true solution of the CPA system exists.

5 Numerical results: validation of CPA

Properties of the effective wave modes predicted by the CPA are compared to those obtained using the effective media random sampling approach in figures 7–9. Attenuation rates are shown in the bottom panels, and the associated energy fluxes are shown in the top panels. Problems involving up to five wave directions are considered.

Results are shown for two single-wave direction problems in figure 7. The problems are identical to those used for figure 2. The left-hand panels are for the problem with an underlying pass-band state, and the right-hand-panels are for the problem with an underlying stop gap state.

The attenuation rates and energy fluxes predicted by the CPA and random sampling are almost identical. However, the following features are noted.
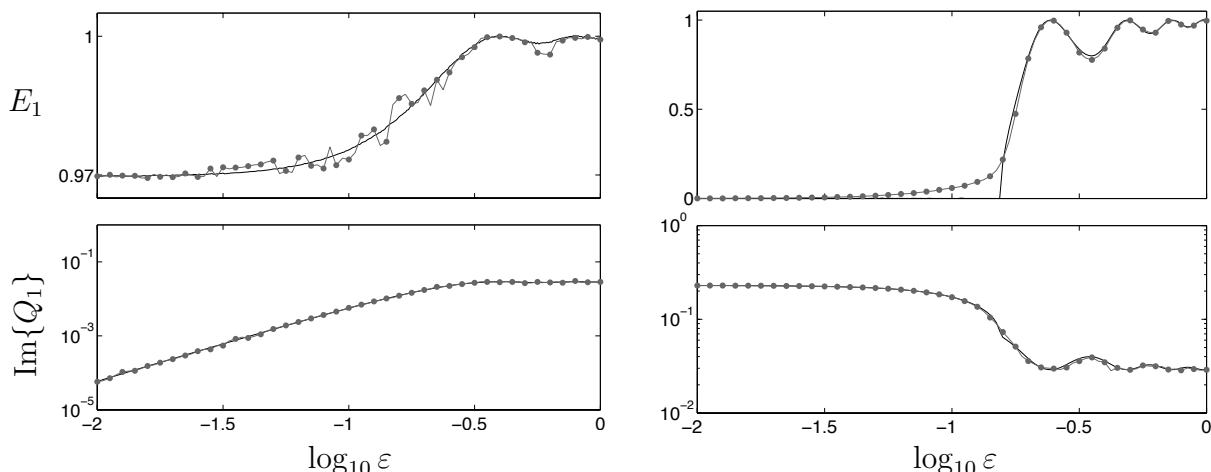
Figure 7: Comparisons of energy fluxes (top panels) and attenuations rates (bottom) produced by the CPA (black curves) and the effective media random sampling approach (grey dotted) for two single-wave problems. The underlying periodic media is in a pass-band state (left-hand panels) and a stop-gap state (right).

(i) Noise exists in the random sampling approximation of the energy flux for the problem with an underlying pass-band state. It is attributed to numerical difficulties in separating modes with small attenuation rates (travelling up and down the array in the one dimensional case).

(ii) A fundamental difference in the approximations exists in the problem involving the underlying stop-gap state. Random sampling predicts a smooth transition between zero energy flux and finite energy flux. Conversely, the CPA predicts a sharp division between the two states. Around this point, a small deviation is also observed between the two approximations of the attenuation rate.

Energy flux is a property of the local wave field, whereas attenuation is an integrated 'global' property of the array. Predictions of energy fluxes are thus expected to be more sensitive than attenuation rates to errors in the approximations.

Comparisons are shown for problems involving two to five wave directions in figures 8–9. The asymmetric two-wave problem previously considered in the bottom right-hand panel of figure 5 is used for the left-hand panels of figure 8. The symmetric three-wave problem previously considered in the right-hand panels of figure 6 are used for right-hand panels. In the three-wave problem, results for the mode that is insensitive to disorder, labelled with subscript 1, are omitted. For zero disorder, both problems possess a mode in a pass-band state and a mode in a stop-gap state.

Results for two problems that have not been considered previously are shown in figure 9. The mean row spacings of the arrays is $kd = 7.5\pi$. In the left-hand panels there are $M = 4$ wave directions and $\psi_0 = 0.1\pi$ is the smallest scattering angle. In the right-hand panels $M = 5$ and $\psi_0 = 0.2\pi$. The in-row spacing of the arrays is $ks = (M - 1)\pi \sec(\psi_0)$. Both problems are therefore symmetric with respect to the y-axis, and both have two pairs of modes that are unaffected by disorder. Values corresponding to these modes are labelled with subscripts 1 and 2, and are omitted from the figures.

Pleasing agreement is observed between the two approximations in all of the multiple-wave problems. Again, the agreement of the attenuation rates is particularly good. Only slight
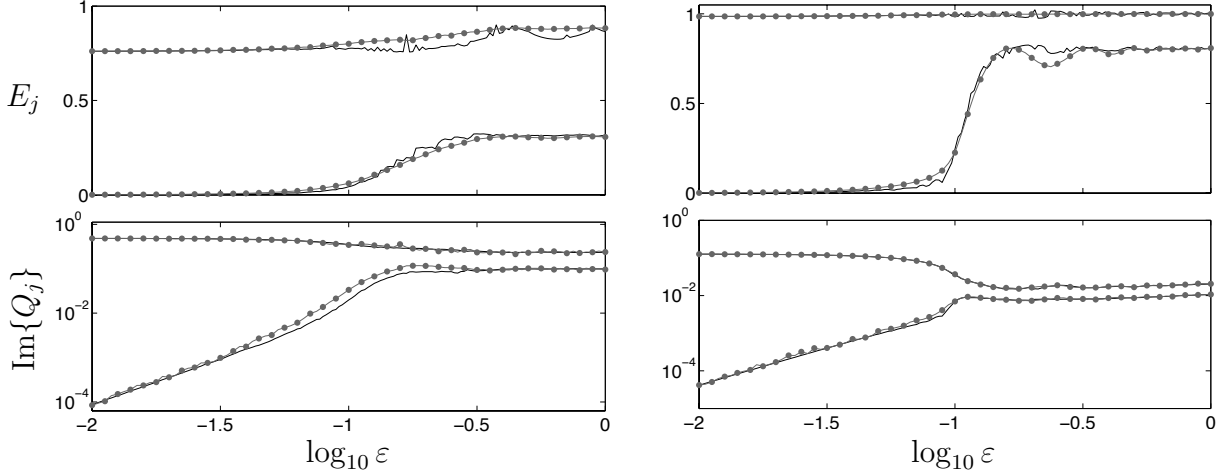
18

Figure 8: As in figure 7, but for two-wave problems ($j = 1, 2$, left-hand panels) and three-wave problems ($j = 2, 3$, right).
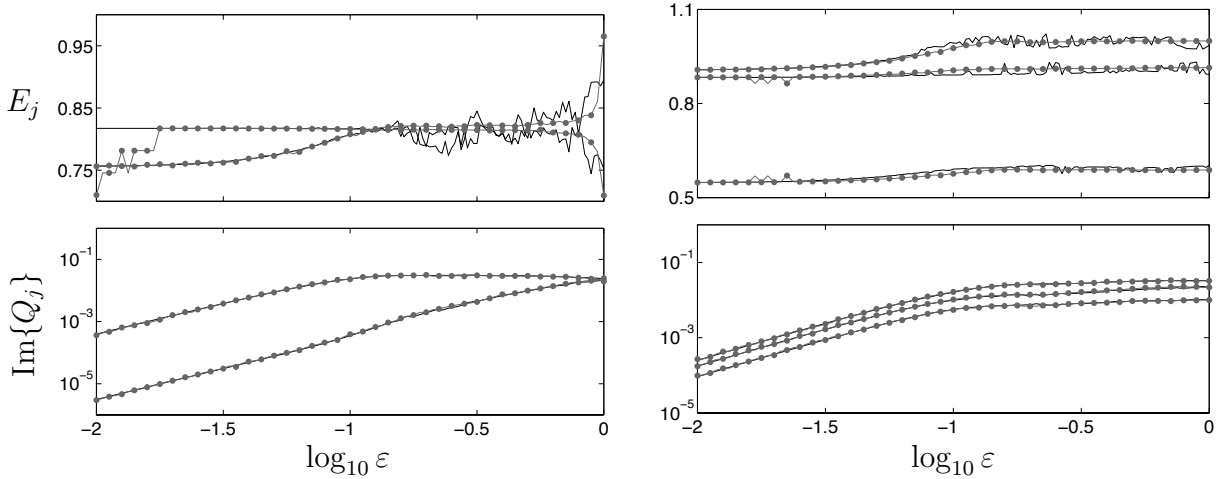

Figure 9: As in figure 7, but for four-wave problems ($j = 3, 4$, left-hand panels) and five-wave problems ($j = 3$–5, right). Values are shown for modes that vary with disorder.

deviations are seen in the two-wave problems in the intervals where a mode transitions from zero energy flux to finite energy flux. Differences in the energy fluxes are typically found in intervals of rapid change, e.g. the oscillations for large disorder in the two-wave problems. Noise is again evident in the random sampling approximation of the energy flux when attenuation rates are small. But, unlike the single-wave problems, noise is evident in the CPA of the energy flux for large disorder. This is attributed to numerical difficulties in solving for the larger systems created by multiple wave directions.

6   Summary and discussion

Wave modes supported by randomly disordered arrays, composed of multiple identical rows of scatterers, were sought using direct numerical approaches and an approximation. Wave interactions between rows were limited to a finite number of propagating waves travelling in known directions. The number of modes supported by the array is equal to the number of wave directions.

In the absence of disorder the arrays are periodic, and the modes can be calculated from the transfer matrix for a single cell in the array. Disorder was introduced in the spacings between the rows. The modal structure of periodic problem was imposed on the disordered problem using ansatzes. The properties of the modes, in particular the array wave numbers, were approximated using random sampling. Two different approaches were adopted. Firstly, a localisation approach, in which the properties were calculated as ensemble averages over a large number of randomly generated realisations. Secondly, an effective media approach, in which the properties are extracted from the ensemble average wave field, calculated from a large number of randomly generated realisations. For both approaches, the modes were decoupled by combining wave fields produced by independent incident waves.

A coherent potential approximation (CPA) was also developed. The CPA predicts the modes from the ensemble average of the scattering properties of a single cell in the array. The CPA assumes that the ensemble average perfectly transmits each of the modes. A numerical algorithm was devised to implement the CPA.

Numerical investigations were conducted (a) to compare the approximations produced by the localisation and effective media approaches, and (b) to validate the CPA using random sampling. The key findings and discussions are listed below.

(i) The two approaches produce the same attenuation rates when the wave interactions are essentially one-dimensional, i.e. one wave direction or two symmetric wave directions. The localisation approach typically requires a smaller ensemble to achieve convergence for large disorder. Conversely, only the effective media approach is able to capture small attenuation rates accurately.

(ii) The attenuation rates produced by the two approaches diverge from one another as the disorder level becomes large for problems involving multiple wave directions. In this regime the coherent wave modes attenuate more rapidly than the modes of the individual wave fields. This indicates that the coherent wave fields do not dominate the attenuation process for large disorder. Every effort has been made to ensure the authenticity of the numerical results presented here. The consistency of the differences between the attenuation rates is a strong indication that the feature is genuine.

(iii) The ensemble average adopted in the localisation approach does not represent phase changes of wave modes supported by the array. For problems in which modes are automatically uncoupled in the individual simulations, i.e. problems involving a single wave direction and significant attenuation, the phase changes associated to local waves travelling up and down the array match those of the effective wave modes attenuating up and down the array, respectively. The methods developed in this study are unable to determine if similar behaviour is present when multiple modes are excited.

(iv) The CPA produces almost identical attenuation rates and energy fluxes as the effective media random sampling approach. This indicates that the CPA is a viable method to capture the modes of an effective wave field in problems involving multiple wave directions.

From a practical standpoint, the CPA proved to be far easier to implement than the random sampling approaches, which are beset with difficulties. The CPA was also more efficient than random sampling for the numerical results presented in this investigation. The attenuation rates predicted by the CPA are robust. However, noise is apparent in the corresponding predictions of energy fluxes for large disorder, which may be caused by the application of a package

minimisation routine. Furthermore, the cost of the minimisation routine does not scale well with respect to the number of wave directions. Therefore, it is unlikely that the CPA algorithm devised here could be applied to problems involving a large number of wave directions, e.g. the multiple-row problem considered by Bennetts [1].

Acknowledgments

Funding

References

[1] L. G. Bennetts. Wave attenuation through multiple rows of scatterers with differing periodicities. *SIAM J. Appl. Maths.*, 71(2):540–558, 2011.

[2] M. V. Berry and S. Klein. Transparent mirrors: rays, waves and localization. *Eur. J. Phys.*, 18:222–228, 1997.

[3] C. M. Linton and P. A. Martin. Semi-infinite arrays of isotropic point scatterers: a unified approach. *SIAM J. Appl. Maths.*, 64(3):1035–1056, 2004.

[4] A. Maurel, P. A. Martin, and V. Pagneux. Effective propagation in a one-dimensional perturbed periodic structure: comparison of several approaches. *Waves Random Complex Media*, 20(4):634–655, 2010.

[5] R. C. McPhedran, L. C. Botten, A. A. Asatryan, N. A. Nicorovici, P. A. Robinson, and C. M. de Sterke. Calculation of electromagnetic properties of regular and random arrays of metalic and dielectric cylinders. *Phys. Rev. E*, 60(6):7614–7617, 1999.

[6] M. A. Peter and M. H. Meylan. Water-wave scattering by vast field of bodies. *SIAM J. Appl. Maths.*, 70(5):1567–1586, 2009.

[7] R. Porter and D. Porter. Interaction of water waves with three-dimensional periodic topography. *J. Fluid Mech.*, 434:301–335, 2001.